

Nanofluidics in the Debye Layer at Hydrophilic and Hydrophobic Surfaces

C. I. Bouzigues,¹ P. Tabeling,^{1,*} and L. Bocquet^{2,3}

¹Laboratoire de Microfluidique, MEMS et Nanostructures, UMR CNRS Gulliver-ESPCI 10, rue Vauquelin 75005 Paris, France

²LPMCN; Université de Lyon; Université Lyon 1 and CNRS, UMR 5586, F-69622 Villeurbanne, France

³Physics Department, Technical University Munich, 85748 Garching, Germany

(Received 15 May 2008; published 9 September 2008)

By using evanescent waves, we study equilibrium and dynamical properties of liquid-solid interfaces in the Debye layer for hydrophilic and hydrophobic surfaces. We measure velocity profiles and nanotracer concentration and diffusion profiles between 20 and 300 nm from the walls in pressure-driven and electro-osmotic flows. We extract electrostatic and zeta potentials and determine hydrodynamic slip lengths with 10 nm accuracy. The spectacular amplification of the zeta potential resulting from hydrodynamic slippage allows us to clarify for the first time the dynamic origin of the zeta potential.

DOI: [10.1103/PhysRevLett.101.114503](https://doi.org/10.1103/PhysRevLett.101.114503)

PACS numbers: 47.61.-k, 47.80.Cb

The development of microfluidics and nanofluidics has raised new challenges to drive and manipulate flows in ever more tiny channels [1,2]. One key question concerns the nature of the boundary condition of fluids at solid surfaces. Recent studies have demonstrated that hydrophobic surfaces develop hydrodynamic slippage at solid surfaces, as quantified by the so-called slip length b [3–5]. Slip lengths on the order of a few tens of nanometers are typically reported for clean hydrophobic surfaces [6–9]. However encouraging, this is insufficient to obtain a substantial decrease of the viscous friction experienced by pressure-driven flows in channels of micrometric size or larger. Increasing slip lengths by orders of magnitude is feasible by patterning the surfaces [10]; nonetheless, with the present state-of-art technology, these surfaces still remain delicate to exploit. The situation is different for electro-osmotic flows, i.e., flows induced by the coupling between surface charges and externally applied electric fields. In this case, it has been theoretically shown [5,11–13] that slip lengths in the nanometric range are sufficient to considerably amplify the electro-osmotic (EO) speeds. This amplification effect is embodied in the surface zeta potential ζ , which enters EO mobility as $\mu_{EO} = \epsilon\zeta/\eta$ (with ϵ the dielectric constant and η the fluid viscosity): Refs. [12,13] predicted that ζ is related to the electrostatic surface potential Ψ_0 , according to $\zeta = \Psi_0(1 + b/\lambda_D)$ where λ_D is the nanometric Debye length characterizing the width of the electric double layer at the surface [14]. This leads accordingly to a $(1 + b/\lambda_D)$ slip-induced amplification factor of ζ . Under realistic conditions, one may obtain a tenfold amplification of the bulk velocity just by increasing the slippage at the wall by a few nanometers. Such a spectacular phenomenon has recently attracted much attention in the context of energy conversion [15]. One may suspect that it plays a role in the development of large zeta potentials consistently observed for hydrophobic surfaces [16,17]; recently, it was used to interpret a number of observations [18]. The theoretical prediction, however

enlightening it could be, has not received an experimental confirmation yet. In this work, we use a total internal reflection fluorescence (TIRF) technique [19,20] to explore simultaneously liquid dynamics and electrostatic potentials between 20 and 300 nm from both hydrophilic and hydrophobic surfaces. The combination of evanescent waves to illuminate the flow, as well as a specific tracking technique and nanometric particles to seed the fluid, allows us to bypass the optical limitations inherent to classical particle velocimetry (PIV) techniques [8,21]. As a result, we bring the first experimental evidence for a slip-induced amplification effect, thus demonstrating that the zeta potential is not a purely electrostatic quantity, but also includes a large contribution originating from hydrodynamic slip.

Throughout the experiments, we used 20 nm sulfate conjugated polystyrene fluorescent particles (Fluospheres, Molecular Probes), seeding ultrapure water (MilliPore, 18.2 M Ω), at a 0.02% concentration. The nanoparticle (NP) surface potential ζ_p was measured by a zetameter apparatus. In our experimental conditions, we measured $\zeta_p = -5.8 \pm 1.2$ mV, corresponding to $q_p = 3.0 \pm 0.6e$ per NP (assuming a thick electrical layer).

Microchannels ($10 \times 100 \mu\text{m}$) are made in polydimethylsiloxane (PDMS) using standard soft lithography techniques [22], and closed by a $170 \mu\text{m}$ thick microscope glass slide. In the case of electro-osmotic flows, a pair of gold electrodes, separated by 2 cm, is deposited onto the glass surface. Flows are either pressure driven or electro-osmotically driven: typical pressure drops are hundreds of Pa, and in the latter, voltages applied across the two electrodes are ~ 10 V. The maximum speeds in the microchannel ranged between 20 and $50 \mu\text{m} \cdot \text{s}^{-1}$. Experiments were performed on a DM-IRM microscope equipped with a $100\times$ NA = 1.46 objective (Leica). Flowing liquid was illuminated by a laser beam (Sapphire 488, Coherent) with a continuously tunable incidence angle θ_i (Fig. 1). Tracers were imaged in a field of view of $80 \times 80 \mu\text{m}$ under

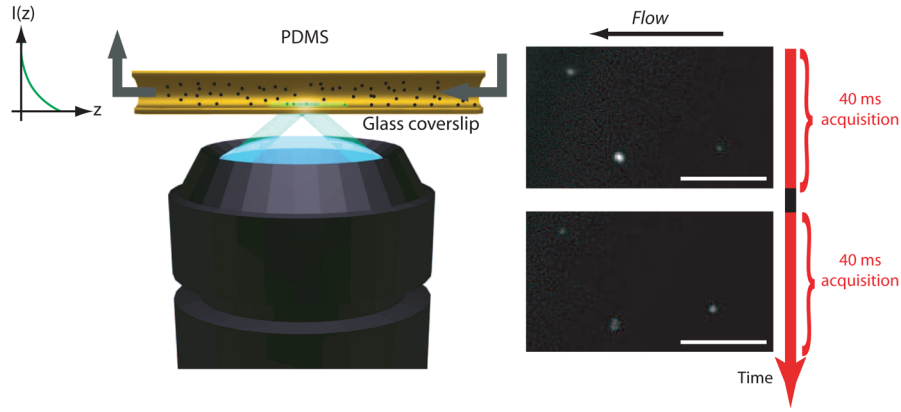


FIG. 1 (color online). Left: Scheme of the TIRF setup. A laser beam is collimated through a high numerical aperture objective ($100\times$ NA = 1.46) with an incidence angle higher than the critical angle for total reflection. Laser is focused in the back focal plane of the objective with an achromatic doublet (focal length 150 mm) and the incidence angle is tunable by a rotating mirror in the optical path. The evanescent wave created within the channel restricts fluorescence to tracers (black dots) in the vicinity of the surface. Right: Typical images obtained by TIRF illumination: the two images are acquired in frame-transfer mode with an exposure/acquisition time of 40 ms. Scale bar represents $5\ \mu\text{m}$.

50 mW illumination on an electron multiplying CCD camera (Ixon Andor) with an acquisition rate of 25 Hz in frame-transfer mode. When θ_i is larger than the critical angle of refraction at a glass-water interface, the illumination power within the channel is given by $I(z) = I_0 \exp(-z/L_e)$, in which L_e is the penetration length. This quantity is determined by measuring the aspect ratio of the laser waist in the sample plane. Under our experimental conditions of TIRF, Fig. 1, L_e was varied between 150 and 400 nm. Given the monodispersity of particle emission (we measured 17% standard type deviation in intensity of tracers on the surface), the fluorescence intensity of a single tracer carries the information on its altitude with an accuracy $\Delta z = L\Delta I/I \sim 17\ \text{nm}$. From the *in situ* measurement of emission intensity of tracers adsorbed on the surface, one determines I_0 and consequently obtains the altitudes of each particle traveling close to the surface.

We performed experiments on hydrophilic and hydrophobic surfaces. Hydrophilic surfaces were prepared by washing Pyrex coverslips with detergent, acetone, toluene, and ethanol. Hydrophobic surfaces were obtained by silanization of the coverslip with octadecyl-trichloro-silane (OTS). Contact angles are $<20^\circ$ (glass) and 95° (OTS) and rms roughnesses measured by atomic force microscopy (AFM) are, respectively, 0.33 ± 0.01 and $0.44 \pm 0.01\ \text{nm}$.

We first discuss measurements of the concentration profiles of NPs as a function of the altitude. The measurements, shown in Fig. 2(a), reveal an exponential depletion of the density of NPs close to the surface [inset of Fig. 2(a)], which can be attributed to electrostatic repulsion between the NPs and the surfaces [23]. The particle distribution at thermal equilibrium is given by $C(z) = C_0 \exp(-q_p \Psi(z)/kT)$, where C_0 is the bulk concentration of the particles and q_p their charge. Using Poisson-Boltzmann description (PB), the electric potential created

by the surface is given by $\Psi(z) = 4k_B T / e \tanh^{-1}[\tanh[e\Psi_0/4k_B T] \exp(-z/\lambda_D)]$, where Ψ_0 is the surface potential and λ_D the Debye length [14]. Experimental profiles are fitted using this expression with both the Debye length and surface energy ($q_p \Psi_0/k_B T$) as free parameters. Predictions for the density profiles are shown in Fig. 2(a), showing good agreement with experiment: we obtain accordingly $\Psi_0 = -69 \pm 20\ \text{mV}$ ($\frac{q_p \Psi_0}{k_B T} = -8.1 \pm 0.9$) for the hydrophilic surface and $\Psi_0 = -65 \pm 19\ \text{mV}$ ($\frac{q_p \Psi_0}{k_B T} = -7.5 \pm 0.7$) for the hydrophobic OTS surface. We checked that the estimated Debye lengths agree with the classical theory for different salt concentrations [14]; see Fig. 2(b). A few remarks are in order. First, the surface potential for the hydrophilic glass and silanized surface are consistent with reported values obtained for the zeta potential on similar surfaces [16,24]. Note that the surface

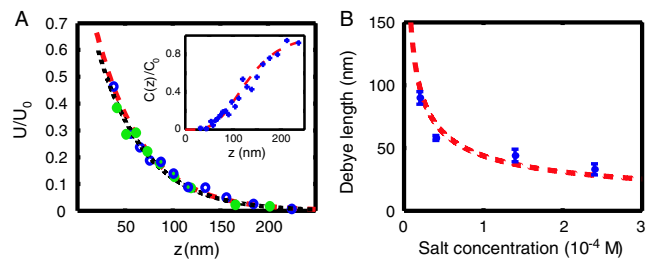


FIG. 2 (color online). (a) Electrostatic interaction energy between NPs and surface, as deduced from the NP concentration profile (see inset): open circles (○), hydrophilic; plain circles (●), hydrophobic. Salt concentration is $1.5 \times 10^{-4}\ \text{mol} \cdot \text{L}^{-1}$. Dashed lines are fits to the PB predictions, providing the Debye length $\lambda_D = 49 \pm 5\ \text{nm}$ and the energy of interaction of the NPs with the surface: $U_0 = 8.1 \pm 0.7 k_B T$ (hydrophilic) and $U_0 = 7.5 \pm 0.7 k_B T$ (hydrophobic). (b) Debye length as a function of salt concentration ρ_{salt} (black dots). The dashed red line is the theoretically expected form, $\lambda_D(\rho_{\text{salt}}) \propto \rho_{\text{salt}}^{-1/2}$ [14].

potentials Ψ_0 refer to the true electrostatic surface potential entering the interaction free energy and not their kinetic counterpart (zeta potential) that will be measured later in the Letter. Surface charge on hydrophobic surfaces is usually attributed to specific adsorption of ions, like OH^- [17].

We now turn to velocity measurements. By using a custom-made algorithm, we track single tracers between two consecutive images. Particles were detected on each image by intercorrelation with the theoretical point spread function of the optical system [25]. Their positions in the plane and intensities were determined by a Gaussian fit of each detected spot, allowing a pointing accuracy of ~ 50 nm. Spots on two consecutive images were associated by computing the likelihood of each spot to be at a given place on the next image. With the small number of particles in the field of view (~ 10 in a $80 \times 80 \mu\text{m}$ field) the association is made unambiguously. Moreover, we restrict ourselves to particles of constant intensity ($\Delta I/I < 20\%$), and use a 25 Hz acquisition frequency on the camera ensuring the particles are always seen. We are then able to guarantee that particles stay in a horizontal plane during the acquisition time. Speed distributions are typically obtained with 1000 particles at each altitude. Such distributions provide both mean velocity and diffusion coefficient profiles between 20 and 300 nm above the surface, with a typical spatial resolution of 30 nm.

Before turning to EO, we consider pressure-driven flows, with the idea of first characterizing slippage effects at the various surfaces. In this case, and for all surfaces, the measured speed profiles $v(z)$ are consistent with a Poiseuille law. In the vicinity of the surfaces, $z \ll w/2$, this predicts $v(z) = 4v_{\text{max}}(z + b)/(w + 4b)$, where v_{max} is the maximum velocity in the channel, w the channel width ($w = 10 \mu\text{m}$), and b the slip length. Velocity profiles in the vicinity of the surfaces are shown in Figs. 3(a) and 3(b). Whereas the measurements agree well with zero-slip expectations in the hydrophilic case, we observed in the case of hydrophobic surfaces a small but systematic deviation from profiles assuming zero slippage at the wall; see Figs. 3(a) and 3(b). In order to estimate slip lengths, we measured independently the maximum speed in the channel v_{max} on the same setup by working in a microPIV mode (i.e., with subcritical angles), thus leaving the slip length b as the only free parameter of the problem. Although the effect of slippage is small [$=\mathcal{O}(b/w)$], this procedure allows us to measure slip lengths with ~ 10 nm accuracy. This yields $b = 3 \pm 7$ nm on hydrophilic glass and $b = 29 \pm 11$ nm on hydrophobic glass. The TIRF setup allows us to complement these velocimetry measurements by streamwise diffusion coefficient D measurements. For particles at a distance z to a surface, the tracer diffusion coefficient is reduced due to hydrodynamic interaction with the surface, according to $D = D_0[1 - \frac{9}{16} \times \{r/(z + b)\}]$ for $z \gg r$ [9,26], where r is the tracer radius and D_0 its bulk diffusion coefficient. The analysis of diffu-

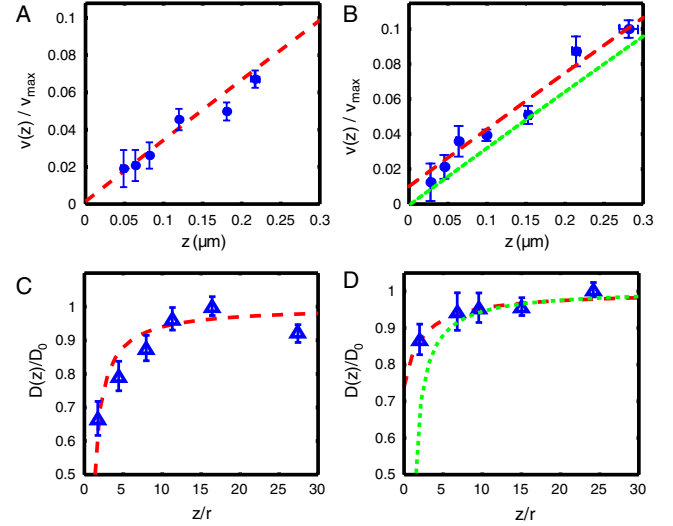


FIG. 3 (color online). Top: Velocity profiles, respectively, above a hydrophilic (a) and OTS-coated (b) glass. Symbols are experimental data and error bar are the uncertainty due to Brownian diffusion. Plain lines are a fit of the normalized data by a Poiseuille law with b as a free parameter. The maximal speed v_{max} and the width of the channel w are experimentally known, leaving the slip length b as the only free parameter: $b = 3 \pm 7$ nm (a) and $b = 29 \pm 11$ nm (b). Bottom: Diffusion coefficient profiles on hydrophilic (c) and OTS-coated (d) glass. Experimental data are the triangles; plain curves are a fit using $D/D_0 = 1 - \frac{9}{16}[r/(z + b)]$ [9,26], where r is the NP radius. This yields is, respectively $b = -3 \pm 7$ nm (a) and $b = 21 \pm 12$ nm (b). Dotted lines in (b)–(d) are predictions with $b = 0$ nm.

sion profiles thus provides an independent determination of the slip length [Figs. 3(c) and 3(d)], yielding $b = -3 \pm 7$ nm, $b = 21 \pm 12$ nm, respectively, for the glass and OTS surfaces, in agreement with those inferred from velocimetry. Altogether, we found no significant slippage on the wetting surface, whereas hydrophobic surfaces have a finite slip length in the tens of nanometer range, consistent with literature data [6,7,9].

We finally come to the main point of this Letter and consider electro-osmotic flows. Velocity profiles for pure electro-osmotic flows (driven by an electric field of 500 V/m) are shown in Fig. 4. These are corrected for the NP diffusiophoretic velocity. A first observation is that a spectacular slippage effect is observed for the hydrophobic surface, in contrast to the hydrophilic one. Comparing with Fig. 3(b), hydrodynamic slip velocities are obviously much stronger for EO than for pressure-driven flows. Second, values of the velocity at infinite distance from the surface define the zeta potential according to $v_{\infty} = -(\epsilon\zeta/\eta)E$ [14]: this gives $\zeta = -66 \pm 8$ mV for the glass surface and $\zeta = -123 \pm 15$ mV for the OTS surface. A key point is that, although surface electrostatic potential Ψ_0 was measured to be similar for hydrophilic and hydrophobic surfaces, the zeta potential is much larger in the hydrophobic case: this is precisely the predicted

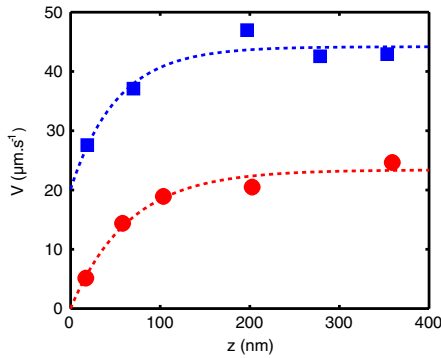


FIG. 4 (color online). Electro-osmotic flows close to hydrophilic glass (●) and hydrophobic OTS (■), corrected for the electrophoretic velocity of the NPs. The deduced zeta potentials are $\zeta = -66 \pm 8$ mV (glass) and $\zeta = -123 \pm 15$ mV (OTS). The salt concentration is 1.5×10^{-4} mol · L⁻¹ and the driving electric field is $E = 500$ V · m⁻¹. Dashed lines are fits to the theoretical predictions using Eq. (1), yielding $\lambda_D = 51 \pm 10$ nm [in agreement with Fig. 2(a)] and $b = 0 \pm 10$ nm (bottom) and $b = 38 \pm 6$ nm (top) for the slip lengths. Note the large slip velocity at the wall in the hydrophobic case, thereby confirming a strong effect of slippage on EO [$= \mathcal{O}(b/\lambda_D)$].

slippage induced amplification effect. Going into more detail, we compare in Fig. 4 the whole velocity profiles with the theoretical expression obtained by solving the coupled PB and Stokes equations with a slip boundary condition at the surface [12,13]. The latter takes the form

$$v(z) = -\frac{\epsilon}{\eta} E [-\Psi(z) + \Psi_0(1 + b\kappa_{\text{eff}})], \quad (1)$$

where $\Psi(z)$ is the PB electrostatic potential given above, and $\kappa_{\text{eff}} = -\Psi'(0)/\Psi_0$ ($\approx \lambda_D^{-1}$) is the surface screening parameter, taking into account nonlinear PB effects. In the comparison with experimental results, we fix surface potential in Eq. (1) to the experimental values for the surface potential Ψ_0 , as obtained from Fig. 2(a), and we leave the slip and Debye length as the only free parameters. The slip lengths from the fitting procedure are $b = 0 \pm 10$ nm (hydrophilic, glass) and $b = 38 \pm 6$ nm (hydrophobic, OTS). These third estimates for the slip lengths are again consistent with the previous two. As observed in Fig. 4, the theoretical expression is in good agreement with the measured velocity profiles, both in the hydrophilic and hydrophobic cases.

These results lead to several important conclusions. On the hydrophilic surface, the zeta potential is indistinguishable from the electrostatic surface potential, $\zeta \approx \Psi_0$, and thereby ζ is representative of the electric properties of the surface. On the hydrophobic surface, the situation is different and we measure $\zeta \approx 2\Psi_0$. This result is in full agreement with the theoretical prediction $\zeta = \Psi_0(1 + \kappa_{\text{eff}}b)$ obtained from Eq. (1) (with, in the present case, $\kappa_{\text{eff}}^{-1} \approx \lambda_D \sim b$). Slippage therefore directly impacts ζ which no longer represents the sole electrostatic properties of the

surface. This result may provide hints for interpreting high ζ potentials measurements obtained with hydrophobic surfaces [16,17].

In conclusion, we report the first detailed velocity profiles obtained between 20 and 300 nm from surfaces for both pressure-driven and electro-osmotic water flows. This exhaustive study allowed us to disentangle for the first time electrostatic from dynamical effects involved in the zeta potential. Our results confirm the strong amplification of the zeta potential by slippage effects, thereby offering a new route to control flows by surface properties.

This work was supported by CNRS, ESPCI, and ANR PNANO.

*patrick.tabeling@espci.fr

- [1] T. Squires and S. Quake, *Rev. Mod. Phys.* **77**, 977 (2005).
- [2] P. Tabeling, *Introduction to Microfluidics* (Oxford University, New York, 2005).
- [3] O.I. Vinogradova, *Int. J. Miner. Process.* **56**, 31 (1999).
- [4] E. Lauga, M. Brenner, and H. Stone, *Handbook of Experimental Fluid Dynamics* (Springer, New York, 2006).
- [5] L. Bocquet and J.-L. Barrat, *Soft Matter* **3**, 685 (2007).
- [6] C.H. Choi, K. Westin, and K. Breuer, *Phys. Fluids* **15**, 2897 (2003).
- [7] C. Cottin-Bizonne *et al.*, *Phys. Rev. Lett.* **94**, 056102 (2005).
- [8] P. Joseph and P. Tabeling, *Phys. Rev. E* **71**, 035303 (2005).
- [9] L. Joly, C. Ybert, and L. Bocquet, *Phys. Rev. Lett.* **96**, 046101 (2006).
- [10] P. Joseph *et al.*, *Phys. Rev. Lett.* **97**, 156104 (2006); C.H. Choi and C. Kim, *ibid.* **96**, 066001 (2006).
- [11] J. Eijkel, *Lab Chip* **7**, 299 (2007).
- [12] V.M. Muller *et al.*, *Colloid J. USSR* **48**, 718 (1986).
- [13] L. Joly *et al.*, *Phys. Rev. Lett.* **93**, 257805 (2004).
- [14] R.J. Hunter, *Foundations of Colloid Science* (Oxford University, Oxford, 2001), 2nd ed.
- [15] Y. Ren and D. Stein, *Nanotechnology* **19**, 195707 (2008).
- [16] R. Schweiss *et al.*, *Langmuir* **17**, 4304 (2001).
- [17] R. Zimmermann *et al.*, *Microfluid. Nanofluid.* **2**, 367 (2006).
- [18] N.V. Churaev, J. Ralston, I.P. Sergeeva, and V.D. Sobolev, *Adv. Colloid Interface Sci.* **96**, 265 (2002).
- [19] P. Huang, J. Guasto, and K. Breuer, *J. Fluid Mech.* **566**, 447 (2006).
- [20] S. Pouya *et al.*, *Exp. Fluids* **39**, 784 (2005).
- [21] S. Devasenathipathy *et al.*, *Exp. Fluids* **34**, 504 (2003).
- [22] J. McDonald *et al.*, *Electrophoresis* **21**, 27 (2000).
- [23] G. Schumacher and T. van de Ven, *Langmuir* **7**, 2028 (1991).
- [24] A. Sze *et al.*, *J. Colloid Interface Sci.* **261**, 402 (2003).
- [25] S. Bonneau, L. Cohen, and M. Dahan, in *Proceedings of the IEEE International Symposium on Biological Imaging, 2005* (IEEE, New York, 2005).
- [26] E. Lauga and T.M. Squires, *Phys. Fluids* **17**, 103102 (2005).